

Formation of Monolithic Nanoporous Copper with Ultrahigh Specific Surface Area through Chemical Dealloying of Mg-Cu Alloy

Wenbo Liu^{1,2,*}, Shichao Zhang^{1,*}, Ning Li², Shenshen An¹, Jiwei Zheng¹

¹ School of Materials Science and Engineering, Beihang University, Beijing 100191, China

² School of Manufacturing Science and Engineering, Sichuan University, Chengdu 610065, China

*E-mail: liuwenbo_8338@163.com; csc@buaa.edu.cn

Received: 25 July 2012 / Accepted: 2 September 2012 / Published: 1 October 2012

The monolithic nanoporous copper (NPC) with ultrahigh specific surface area can be achieved through chemical dealloying of melt-spun Mg 12 at.% Cu alloy comprising α -Mg and Mg₂Cu phases in an acidic solution at room temperature. The microstructure of the monolithic NPC ribbons was characterized using X-ray diffraction, scanning electron microscopy, energy dispersive X-ray analysis, transmission electron microscopy, and high-resolution transmission electron microscopy. The experimental results show that the melt-spun Mg 12 at.% Cu alloy can be totally dealloyed, resulting in the formation of uniform-structured NPC ribbons with relatively large pore sizes compared with that of ligament dimensions. This can be well explained as a consequence of a combination of the synergetic dealloying of α -Mg and Mg₂Cu in the dual-phase Mg-Cu alloy and the fast surface diffusion of Cu atoms along alloy/solution interfaces during dealloying. Meanwhile, we found cracking to be unavoidable in the as-dealloyed samples, indicating the 12 at.% Cu content in the Mg-Cu alloy system is the lowest limit of Cu concentration to obtain the monolithic NPC, below which cracks will extend fast causing the collapse of porous structures. Based upon its special structure features, the Brunauer-Emmett-Teller (BET) surface area of the monolithic NPC is much high and can be determined to be $34.7 \pm 0.1 \text{ m}^2 \text{ g}^{-1}$, which would be especially beneficial for sensing and actuating applications.

Keywords: Monolithic nanoporous copper; Dealloying; Mg-Cu alloy; BET surface area; Surface diffusion

1. INTRODUCTION

Nanoporous metals (NPMs), as novel functional materials, have recently attracted considerable interest in a wide variety of applications including catalysis, sensors, actuators, fuel cells, microfluidic flow controllers, and so forth [1-4]. Since it has been found that chemical/electrochemical dealloying

can be used to yield a broad range of porous metals, during the latest decades, a great deal of effort has been directed towards the investigation of NPMs prepared through dealloying [5-9]. Currently, investigations of NPMs have been mainly focused on synthesis. Typically, fabrication of porous metals with large specific surface areas would be especially beneficial for sensing and actuating applications; meanwhile, the mechanical integrity of porous metals is of great importance in these applications because uniformity and continuity are also key requirements [10-12]. For these reasons, the widespread use of dealloying technique to make monolithic NPMs with large surface areas urgently needs to be investigated.

Wang et al. [13] have reported that monolithic nanoporous silver (NPS) with coarse ligament/channel sizes (more than 100 nm) and BET specific surface area of $1.6 \pm 0.1 \text{ m}^2 \text{ g}^{-1}$ can be synthesized from melt-spun Al 25 at.% Ag alloy by chemical dealloying in an acidic solution. It is worthwhile noting that, however, such a low specific surface area would be not enough favorable for their applications such as in sensing. Zhang et al. [14] also claimed monolithic nanoporous palladium (NPP) can be achieved by dealloying of rapid solidified Al 20 at.% Pd alloy in the 5wt.% HCl solution, which possesses an improved BET surface area, $7.4 \pm 0.1 \text{ m}^2 \text{ g}^{-1}$. Recently, our group also developed a series of effective dealloying routes to fabricate monolithic NPMs with large surface areas through one-pot chemical dealloying of multi-phase alloy systems, in which a significantly high value, $23.4 \pm 0.1 \text{ m}^2 \text{ g}^{-1}$, can be reached as comparison with those reports in the literatures [15-18]. In view of their applications in broader fields, it is our constant aim to further synthesize monolithic NPMs with larger specific surface areas through dealloying. From this perspective, Mg-Cu alloy herein was taken as an example to synthesize monolithic NPC with ultrahigh specific surface area through rapid solidification and chemical dealloying. The results show that the melt-spun Mg 12 at.% Cu alloy can be fully dealloyed and results in the formation of monolithic NPC with an ultrahigh BET surface area of $34.7 \pm 0.1 \text{ m}^2 \text{ g}^{-1}$, which would be especially beneficial for sensing and actuating applications. Additionally, it can be found cracking to be unavoidable in the as-dealloyed samples, suggesting the 12 at.% Cu content in the Mg-Cu alloy system is the lowest limit of Cu concentration, below which monolithic NPC could not be obtained. Based on our current understanding of dealloying process, the corresponding mechanism is discussed in detail.

2. EXPERIMENTAL SECTION

Mg-Cu alloy with nominal composition of 12 at.% Cu was prepared from pure Mg (99.9 wt.%) and pure Cu (99.999 wt.%). Voltaic arc heating was employed to melt the charges in a copper crucible under an argon atmosphere, and then the melt was cooled down into ingots in situ. By use of a single roller melt spinning apparatus, the ingots were remelted in a quartz tube by high-frequency induction heating and then melt-spun onto a copper roller at a circumferential speed of ~3000 rpm in a controlled argon atmosphere. The ribbons obtained were typically 20-40 μm in thickness, 4-6 mm in width, and several centimeters in length. The dealloying of the rapid solidified Mg-Cu ribbons was performed in a 1 wt.% HCl aqueous solution at room temperature (RT) until no obvious bubbles emerged. After

dealloying, the samples were rinsed with distilled water and dehydrated alcohol. The as-dealloyed samples were kept in a vacuum chamber to avoid oxidation.

Microstructural characterization and analysis of the melt-spun alloy ribbons and as-dealloyed samples were made using X-ray diffraction (XRD, Rigaku D/Max-2400) with Cu K α radiation, scanning electron microscopy (FESEM, Hitachi S-4800) with an energy dispersive X-ray (EDX) analyzer, transmission electron microscopy (TEM, JEOL JEM 2100F) with selected-area electron diffraction (SAED), and high-resolution transmission electron microscopy (HRTEM, JEOL JEM 2100F). To test the electrochemical activities of α -Mg and Mg₂Cu phases in the melt-spun Mg-Cu alloy, potentiodynamic polarizations studies were conducted on single-phase α -Mg solid solution and Mg₂Cu intermetallics in the 1 wt.% HCl solution at RT by using an electrochemical measurement unit (PARSTAT 2273). The experiments were carried out in a standard three-electrode electrochemical cell (200mL) with a Pt plate electrode as a counter electrode, a saturated calomel electrode (SCE) as a reference electrode, and the alloy ribbon as the working electrode. Polarization scan was performed towards positive values at a scan rate of 1.0 mV s⁻¹, after allowing a steady state potential to develop. In order to evaluate specific surface areas of the as-dealloyed samples, the N₂ adsorption/desorption experiments were carried out at 77 K on a Nova Station A automatic surface area and pore radius distribution apparatus.

3. RESULTS AND DISCUSSION

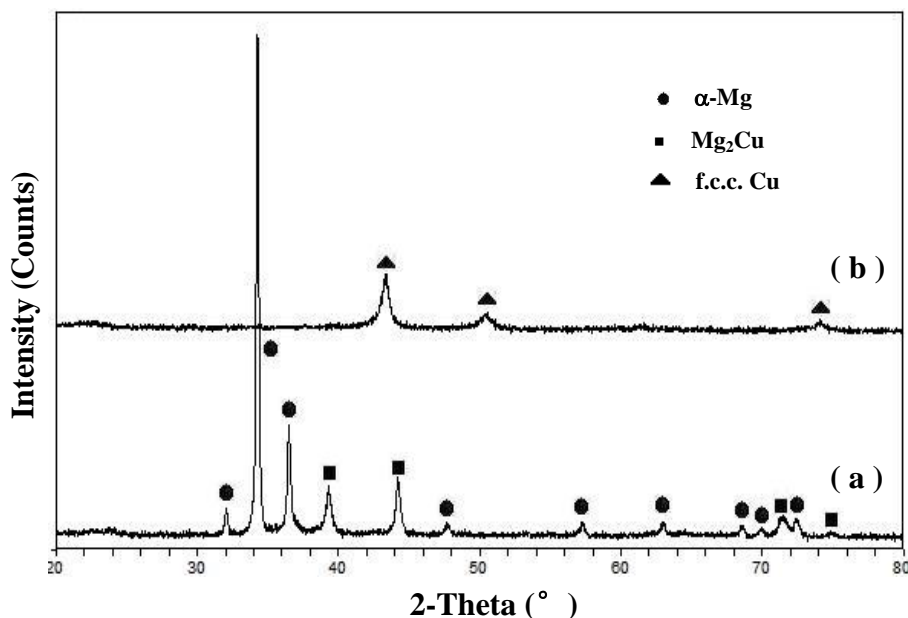


Figure 1. XRD patterns of melt-spun Mg 12 at.% Cu alloy ribbons (a) before and (b) upon dealloying in the 1 wt.% HCl solution at RT.

Figure 1 shows the XRD patterns of the starting melt-spun Mg 12 at.% Cu alloy and the as-dealloyed samples upon dealloying in the HCl solution, respectively. The filled circles, squares and

triangles stand for α -Mg, Mg_2Cu and Cu, respectively. The Mg 12 at.% Cu alloy is composed of two distinct phases: α -Mg and Mg_2Cu (Figure 1a), while the amount of α -Mg phase is slightly dominant than that of Mg_2Cu in the alloy. Upon dealloying, only a face-centered cubic (f.c.c.) Cu phase can be identified in the as-dealloyed samples (Figure 1b).

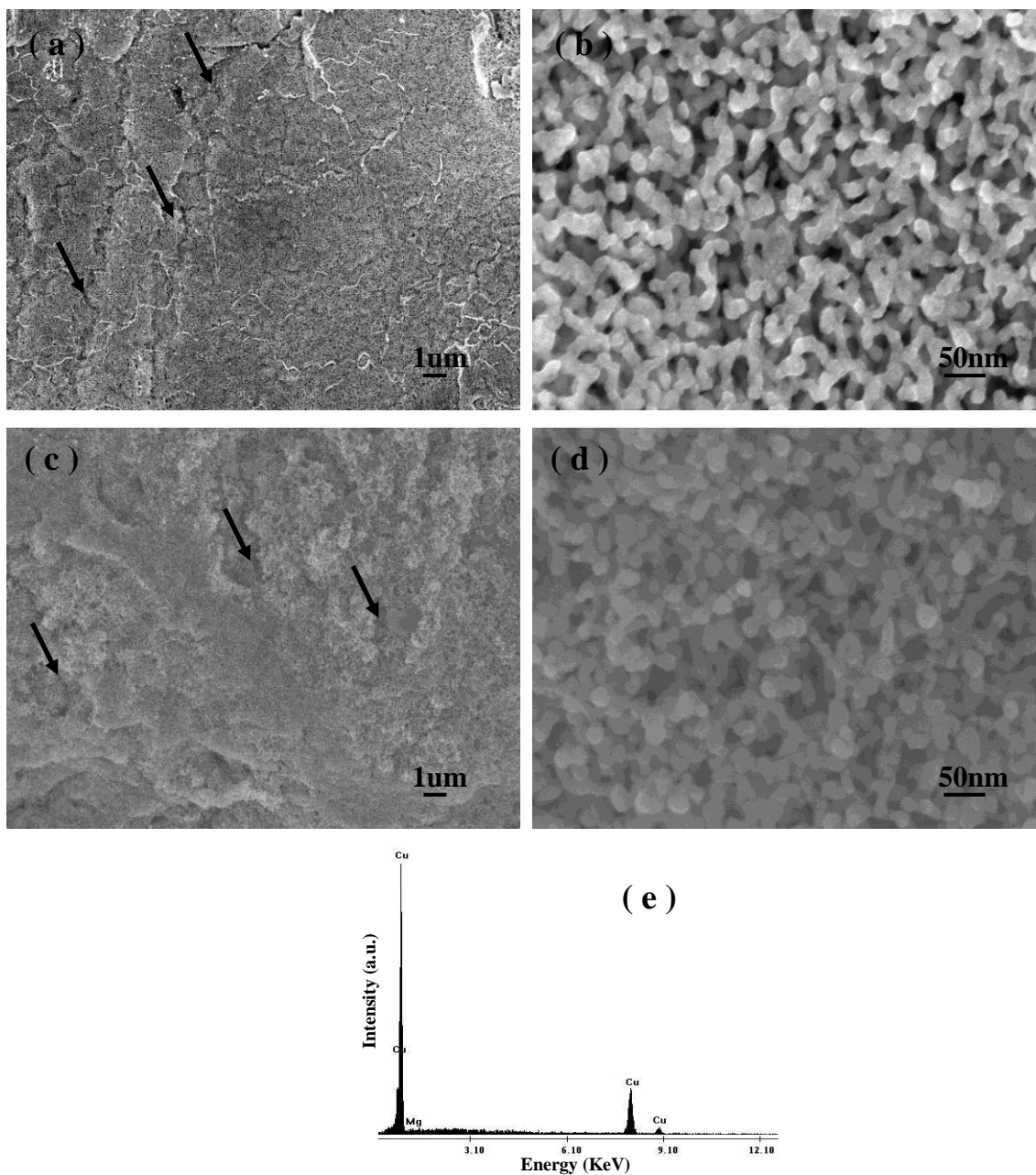


Figure 2. SEM images showing the microstructure of the monolithic NPC by dealloying in the 1 wt.% HCl solution at RT. Parts a and b are the plane views; parts c and d are the section views. Parts a and c show the SEM images at lower magnifications, in which arrows denote the typical sites of cracks. (e) EDX spectrum of monolithic NPC by dealloying of the Mg 12 at.% Cu alloy. a.u.: arbitrary units.

Figure 2 shows the microstructure of monolithic NPC upon dealloying of the Mg 12 at.% Cu alloy in the HCl solution. It is clear that the as-dealloyed samples exhibit an open, three-dimensional (3D) bicontinuous interpenetrating ligament-pore structure with relatively large pore sizes of 100 ± 20 nm as comparison with that of ligament dimensions (20 ± 5 nm). Moreover, we found cracking to be unavoidable in the as-dealloyed samples, especially in the SEM images at low magnifications as marked by some arrows in Figure 2a and 2c. EDX analysis has been performed on the NPC ribbons, and one typical spectrum is shown in Figure 2e. It is obvious that only Cu can be identified and all of Mg is removed from the Mg-Cu alloy during dealloying. In contrast, NPG by dealloying of Ag-Au alloys normally contains some at.% residual Ag. The residual Ag is expected to be trapped inside the Au ligaments based on the dealloying mechanism [19-20]. Also, the residual Ag cannot be totally removed but asymptotically reaches a limit at exhaustively long etching times (up to 100 h) [19].

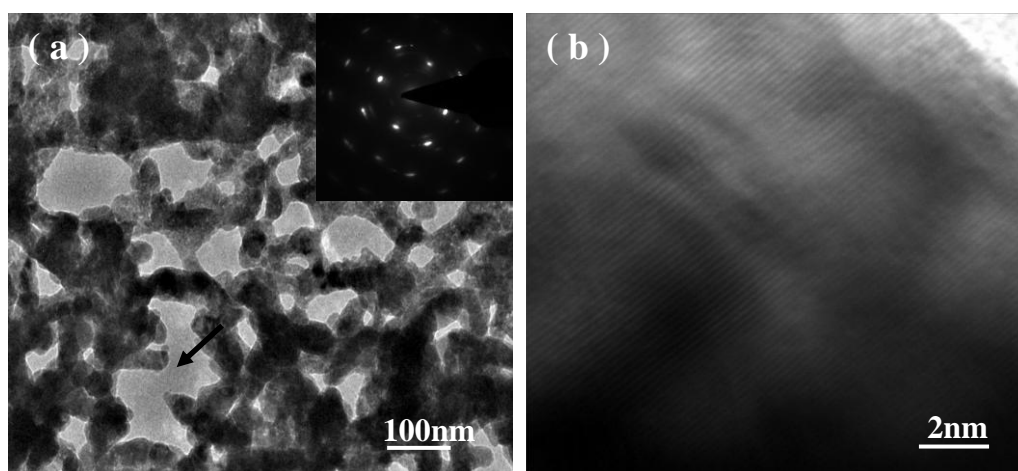


Figure 3. (a) TEM image showing the porous structure of the monolithic NPC ribbons by dealloying of the Mg 12 at.% Cu alloy in the 1 wt.% HCl solution at RT, in which the arrow denotes a typical cracking site. (Inset) SAED pattern corresponding to the ligament in part a. (b) HRTEM image shows lattice fringes extending throughout the whole ligament.

In addition, TEM observation further verifies the porous structure and local cracking of the monolithic NPC ribbons and one typical TEM bright-field image is shown in Figure 3a. A SAED pattern of one ligament shows a hexagonal pattern, which is from the f.c.c. Cu [110] zone axis, indicating a single crystalline characteristic of the selected area (inset of Figure 3a). Moreover, lattice fringes extending throughout the whole ligament (Figure 3b) can further verify the single crystal nature of the ligament in the NPC. It should be noted, however, the present results are essentially different from the established notion that the crystal lattice orientation is retained during dealloying of Ag-Au alloys with the conservation of the grain size of the master alloys [21-24]. For the lattice structure of the resulting NPC is considerably different from that of Mg_2Cu in the initial Mg-Cu alloy (Mg_2Cu : face-centered orthorhombic; Cu: f.c.c.).

Figure 4 shows Tafel polarization curves of single-phase α -Mg solid solution and Mg_2Cu intermetallics in the HCl solution at RT, respectively. It can be found that the difference between

corrosion potentials of the single-phase α -Mg and Mg_2Cu in the acidic solution is ~ 793 mV(SCE), which clearly indicates that the α -Mg has a relatively high electrochemical activity compared to the Mg_2Cu in the HCl solution.

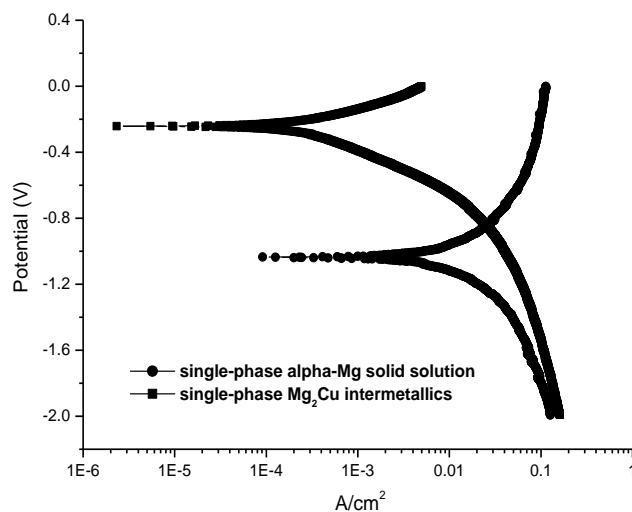


Figure 4. Tafel polarization curves of single-phase α -Mg solid solution and Mg_2Cu intermetallics in the HCl solution at RT.

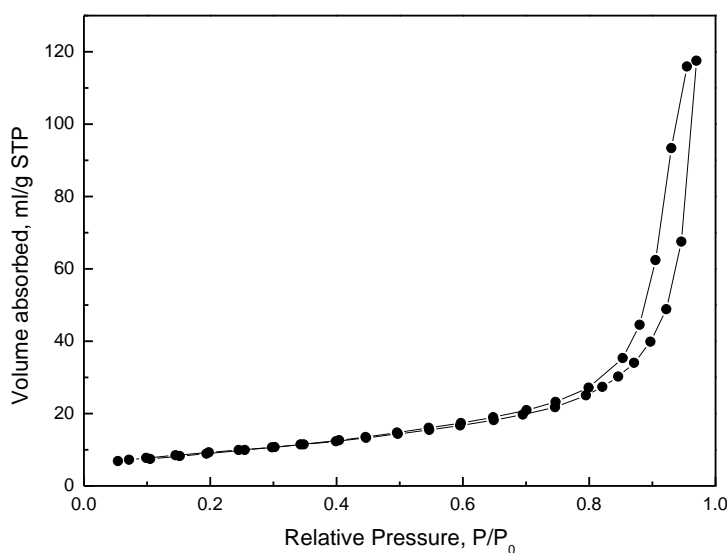


Figure 5. N₂ isotherms at 77 K for the monolithic NPC ribbons by dealloying of the melt-spun Mg 12 at.% Cu alloy in the HCl solution at RT.

The specific surface areas of the resultant porous products can be evaluated based upon N₂ adsorption/desorption experiments. Figure 5 shows the N₂ adsorption/desorption isotherms for the monolithic NPC ribbons by dealloying of the melt-spun Mg 12 at.% Cu alloy in the 1 wt.% HCl solution. The result shows that the BET surface area of the appointed NPC is ultrahigh and has been

determined to be $34.7 \pm 0.1 \text{ m}^2 \text{ g}^{-1}$, which would be especially beneficial for sensing and actuating applications.

It is generally recognized that ideal bicontinuous nanoporous structures are obtained from binary alloy families with a single-phase solid solubility across all compositions by chemical/electrochemical dealloying. The formation mechanism of nanoporous structures during dealloying has been described in the literature [5]. It has been shown that ligaments form as a result of an intrinsic pattern formation during which aggregation of chemically driven noble metal atoms occurs. The process started with selective dissolution of base metal atoms from the outermost alloy surface, leaving behind noble metal atoms that diffused along alloy/solution interfaces and agglomerated into the ligaments. Thus, porosity evolution forms dynamically during dissolution and is not due to one active component simply being excavated out of a binary alloy [25].

However, if multiple phases exist in an alloy, a more complicated process will occur during dealloying. Typically, in a dual-phase alloy, if one phase can be dealloyed and another not, the alloy can be used to fabricate nanoporous metal composites, while if one phase is entirely dissolved and another is partly corroded, the dealloying of the alloy can lead to the formation of NPMs with bimodal channel size distributions [26,27]. In this case, the present Mg 12 at.% Cu alloy is composed of α -Mg and Mg_2Cu phases. According to the non-equilibrium solidification theory, during the rapid solidification of the Mg-Cu alloy, eutectics of α -Mg and Mg_2Cu phases can directly nucleate and continually grow from the initial liquid, suppressing the precipitation of primary α -Mg phase due to the fast cooling rate, characteristic of a two-phase bicontinuous microstructure. During the etching, the excavation of α -Mg phase out of the alloy could contribute to the formation of large-sized channels in the NPC, while the dealloying of Mg_2Cu phase would result in the nanoporous structure of the large-sized channel walls. Thus, it would be reasonable to assume that the dealloying of the melt-spun Mg 12 at.% Cu alloy could result in the formation of NPC with bimodal channel size distributions, comparable to the case for NPG with bimodal channel size distributions in the literature [28]. Intriguingly, in actual fact, unlike the bimodal morphology of the NPG from the Al-Au alloy composed of two phases: α -Al and Al_2Au [28], the microstructure of NPC from the present Mg 12 at.% Cu alloy is homogeneous throughout the whole ribbons although the initial alloy also contains similar-typed two phases: α -Mg and Mg_2Cu . We consider that just the synergetic dealloying of the α -Mg and Mg_2Cu in the dual-phase Mg-Cu alloy and the fast surface diffusion of Cu atoms along the alloy/solution interfaces result in the formation of resulting NPC with a homogeneous porous structure. For the present Mg 12 at.% Cu alloy, the electrochemical activity of α -Mg phase is much higher than that of Mg_2Cu as indicated in Figure 4. Thus, α -Mg and Mg_2Cu phases existing in the alloy can form corrosion couple cells, with the α -Mg (Mg-rich phase) acting as an anode and preferentially dissolving compared to the Mg_2Cu . The preferential dissolution of α -Mg phase forms a large number of tiny paths like a 3D porous network for the penetration of the solution throughout the whole thickness of the ribbons and the dealloying of α -Mg facilitates that of Mg_2Cu . For the Mg_2Cu phase, Mg can be selectively etched, leaving behind Cu atoms diffusing along the alloy/solution interfaces and eventually agglomerating into the ligaments. Recently, Wang et al. [13] also have reported that the synergetic dealloying of α -Al and Ag_2Al in the dual-phase Al-Ag alloy and the fast surface diffusion of Ag atoms can lead to the formation of NPS with a homogeneous porous structure. Obviously, the

surface diffusivity of Cu in solution is on the order of $10^{-10} \text{ cm}^2 \cdot \text{s}^{-1}$, faster than that of Ag (on the order of $10^{-12} \text{ cm}^2 \cdot \text{s}^{-1}$), and much faster than that of Au (on the order of $10^{-14} \text{ cm}^2 \cdot \text{s}^{-1}$) [13,29]. Thus, it may be easier to understand that the synergetic dealloying of α -Mg and Mg_2Cu in the dual-phase Mg-Cu alloy and the faster surface diffusion of Cu atoms should be responsible for the uniformity of the resultant nanoporous products.

Moreover, both high surface area and good mechanical integrity of NPMs are of considerable importance for their wide applications, such as in sensing and actuating fields. Based upon the binary Mg-Cu alloy phase diagram [30], it can be known that with the decrease of Cu content in the initial alloys, the volume fraction of the α -Mg phase continually increases, while a corresponding decrease takes place in the Mg_2Cu . In the present Mg 12 at.% Cu alloy, just the low amount of Mg_2Cu phase results in the relatively small length scales of ligaments compared to that of pore dimensions in the resultant NPC due to its dependence on the Cu content in the Mg_2Cu . Obviously, it is quite beneficial for the enhancement of specific surface area of NPC. However, it is worthwhile noting cracking to be unavoidable in the as-dealloyed samples, indicating the 12 at.% Cu for the dealloying of Mg-Cu alloy family in the HCl solution is the lowest limit of Cu concentration, below which the porous structures will collapse and the shape of the monolith cannot be preserved due to the fast extension of cracks. For example, the dealloying of a melt-spun Mg 10 at.% Cu alloy results in the formation of NPC powders (like Raney metals [31]) instead of monolithic ribbons (not shown here). Therefore, we can conclude that in the Mg-Cu alloy system, monolithic NPC with largest specific surface area can be obtained from the dealloying of Mg-Cu alloy with 12 at.% Cu in the HCl solution.

Based on our present work, it can be proposed that one can employ this simple and effective approach to obtain monolithic NPC with ultrahigh specific surface area from Mg-Cu alloy system. Moreover, it will have important implications for understanding the underlying physical mechanism of dealloying of multi-phase alloys, fabricating novel NPMs with larger specific surface areas from other multi-phase alloy families, and further exploring their promising applications in broader fields, such as sensors, actuators, and lithium ion batteries. Some encouraging test findings have been obtained in our previous work [32-34], the extensive study is in progress.

4. CONCLUSION

In summary, monolithic NPC ribbons with ultrahigh specific surface area can be fabricated through chemical dealloying of melt-spun Mg 12 at.% Cu alloy comprising α -Mg and Mg_2Cu phases in the HCl solution at room temperature. The dual-phase Mg 12 at.% Cu alloy can be fully dealloyed, resulting in the formation of uniform-structured NPC ribbons with relatively large pore sizes compared to that of ligament dimensions. This can be attributed to the synergetic dealloying of α -Mg and Mg_2Cu in the dual-phase Mg-Cu alloy and the fast surface diffusion of Cu atoms along alloy/solution interfaces during dealloying. Additionally, it can be found cracking to be unavoidable in the as-dealloyed samples, indicating monolithic NPC cannot be obtained from Mg-Cu alloys with copper contents below 12 at.% due to the fast extension of cracks. The BET surface area of the monolithic

NPC is much high and can be determined to be $34.7 \pm 0.1 \text{ m}^2 \text{ g}^{-1}$, which would be especially beneficial for sensing and actuating applications.

ACKNOWLEDGEMENT

We give thanks to financial support by the State Key Basic Research Program of PRC (2007CB936502), the National Natural Science Foundation of China (50574008, 50954005, 51074011), the National 863 Program Project (2006AA03Z230, 2008AA03Z208), the China Postdoctoral Science Foundation Funded Project (2011M500214), the Basic Research Fund Project of Beihang University (501LJJC2012101001), and the Shanghai Aerospace Science and Technology Innovation Fund Project (SAST201269). Also, we are grateful to Prof. T. Zhang and Dr. J.F. Wang for assistance in preparation of the initial alloy ribbons.

References

1. G. C. Bond and D. T. Thompson, *Catal. Rev.*, 41 (1999) 319.
2. T. You, O. Niwa, M. Tomita and S. Hirono, *Anal. Chem.*, 75 (2003) 2080.
3. J. R. Weissmueller, N. Viswanath, D. Kramer, P. Zimmer, R. Wuerschum and H. Gleiter, *Science*, 300 (2003) 312.
4. S. H. Joo, S. J. Choi, K. J. Kwa and Z. Liu, *Nature*, 412 (2001) 169.
5. J. Erlebacher, M. J. Aziz, A. Karma, N. Dimitrov and K. Sieradzki, *Nature*, 410 (2001) 450.
6. W. B. Liu, S. C. Zhang, N. Li, J. W. Zheng and Y. L. Xing, *J. Electrochem. Soc.*, 157 (2010) D666.
7. M. Stratmann and M. Rohwerder, *Nature*, 410 (2001) 420.
8. W. B. Liu, S. C. Zhang, N. Li, J. W. Zheng and Y. L. Xing, *Corrosion Sci.*, 53 (2011) 809.
9. W. B. Liu, S. C. Zhang, N. Li, J. W. Zheng and Y. L. Xing, *J. Electrochem. Soc.*, 158 (2011) D91.
10. Y. Ding and J. Erlebacher, *J. Am. Chem. Soc.*, 125 (2003) 7772.
11. W. B. Liu, S. C. Zhang, N. Li, J. W. Zheng and Y. L. Xing, *Microporous Mesoporous Mater.*, 138 (2011) 1.
12. H. J. Jin, X. L. Wang, S. Parida, K. Wang, M. Seo and J. Weissmuller, *Nano Lett.*, 10 (2010) 187.
13. X. G. Wang, Z. Qi, C. C. Zhao, W. M. Wang and Z. H. Zhang, *J. Phys. Chem. C*, 113 (2009) 13139.
14. Z. H. Zhang, Y. Wang, Z. Qi, W. H. Zhang, J. Y. Qin and J. Frenzel, *J. Phys. Chem. C*, 113 (2009) 12629.
15. W. B. Liu, S. C. Zhang, N. Li, J. W. Zheng, S. S. An and Y. L. Xing, *Int. J. Electrochem. Sci.*, 7 (2012) 6365.
16. W. B. Liu, S. C. Zhang, N. Li, J. W. Zheng, S. S. An and Y. L. Xing, *Int. J. Electrochem. Sci.*, 7 (2012) 2240.
17. W. B. Liu, S. C. Zhang, N. Li, J. W. Zheng and Y. L. Xing, *J. Electrochem. Soc.*, 158 (2011) D611.
18. W. B. Liu, S. C. Zhang, N. Li, J. W. Zheng, S. S. An and Y. L. Xing, *Corrosion Sci.*, 58 (2012) 133.
19. M. C. Dixon, T. A. Daniel, M. Hieda, D. M. Smilgies, M. H. W. Chan and D. L. Allara, *Langmuir*, 23 (2007) 2414.
20. K. Sieradzki, R. R. Corderman and K. Shukla, *Phil. Mag. A*, 59 (1989) 713.
21. Y. Ding, A. Mathur, M. W. Chen and J. Erlebacher, *Angew. Chem., Int. Ed.*, 44 (2005) 4002.
22. Y. Ding, Y. J. Kim and J. Erlebacher, *Adv. Mater.*, 16 (2004) 1897.
23. S. Parida, D. Kramer, C. A. Volkert, H. Rösner, J. Erlebacher and J. Weissmüller, *Phys. Rev. Lett.*, 97 (2006) 035504.
24. A. J. Forty and P. Durkin, *Philos. Mag. A*, 42 (1980) 295.
25. J. Erlebacher, *J. Electrochem. Soc.*, 151 (2004) C614.

26. Z. Qi, C. C. Zhao, X. G. Wang, J. K. Lin, W. Shao, Z. H. Zhang and X. F. Bian, *J. Phys. Chem. C*, 113 (2009) 6694.
27. W. B. Liu, S. C. Zhang, N. Li, J. W. Zheng and Y. L. Xing, *Int. J. Electrochem. Sci.*, 6 (2011) 5445.
28. Z. H. Zhang, Y. Wang, Z. Qi, J. K. Lin and X. F. Bian, *J. Phys. Chem. C*, 113 (2009) 1308.
29. N. Hirai, H. Tanaka and S. Hara, *Appl. Surf. Sci.*, 506 (1998) 130.
30. T. B. Massalski, J. L. Murray, L. H. Bennett and H. Baker, *American Society for Metals*, Ohio, (1986).
31. M. Raney, *U.S. Patent* No. 1563587, (1925).
32. S. C. Zhang, Y. L. Xing, W. B. Liu and J. W. Zheng, *The 15th International Meeting on Lithium Batteries, IMLB*, J. Electrochem. Soc., Abstract #82, Montréal, Canada, June 27-July 2, 2010.
33. J. W. Zheng, S. C. Zhang, W. B. Liu, Y. L. Xing and Z. J. Du, *J. New Mat. Electrochem. Systems*, 14 (2011) 213.
34. W. B. Liu, S. C. Zhang, J. W. Zheng and Y. L. Xing, *The 4th international conference on advanced lithium batteries for automobile application, ABAA-4*, Tianjin Institute of Power Sources & China Industrial Association of Power Sources, Abstract #108, Beijing, China, September 21-23, 2011.